SIAM J. APPL. MATH.
Vol. 80, No. 3, pp. 1083–1100

HIDDEN ASYMPTOTIC SYMMETRY IN A LONG ELASTIC STRUCTURE*

SHRINIDHI S. PANDURANGI†, TIMOTHY J. HEALEY‡, AND NICOLAS TRIANTAFYLLIDIS§

Abstract. Transverse wrinkles are known to appear in thin rectangular elastic sheets when stretched in the long direction. Numerically computed bifurcation diagrams for extremely thin, highly stretched films indicate entire orbits of wrinkling solutions; cf. Healey, Li, and Cheng [J. Nonlinear Sci., 23 (2013), pp. 777–805]. These correspond to arbitrary phase shifts of the wrinkled pattern in the transverse direction. While such behavior is normally associated with problems in the presence of a continuous symmetry group, an unloaded rectangular sheet possesses only a finite symmetry group. In order to understand this phenomenon, we consider a simpler problem more amenable to analysis—a finite-length beam on a nonlinear softening foundation under axial compression. We first obtain asymptotic results via amplitude equations that are valid as a certain nondimensional beam length becomes sufficiently large. We deduce that any two phase shifts of a solution differ from one another by exponentially small terms in that length. We validate this observation with numerical computations, indicating the presence of solution orbits for sufficiently long beams. We refer to this as "hidden asymptotic symmetry."

Key words. asymptotic analysis, bifurcation, hidden symmetry, beam-foundation system

AMS subject classifications. 74B20, 74G10, 74G60

DOI. 10.1137/19M125162X

1. Introduction.

We address a question in this work that was previously raised in the context of wrinkling in highly stretched thin elastic membranes [1]. When a rectangular sheet, say, of length L and width W, with $L > W$, is uniaxially stretched between rigid end grips in the longer direction, transverse wrinkles often emerge. The phenomenon is well known, e.g., [2, 3, 4, 5]. The question in [1] concerns observed properties of computed transverse wrinkling patterns. Finite-element solutions were obtained on half of the domain, of width $W/2$, for two distinct cases, assuming (1) reflection symmetry leading to symmetric boundary conditions along the cut edge; (2) reflection-inversion symmetry leading to anti-symmetric boundary conditions there. The two boundary value problems give rise to transverse wrinkled patterns that are (1) even and (2) odd, respectively, about the mid-plane. Remarkably the two resulting global bifurcation diagrams are identical (to within several significant digits commensurate with the accuracy of the computations); cf. [1]. Additional computations were

*Received by the editors March 21, 2019; accepted for publication (in revised form) February 19, 2020; published electronically May 4, 2020.
https://doi.org/10.1137/19M125162X

Funding: This work was supported in part by grants from École Polytechnique and C.N.R.S. (Centre National de Recherche Scientifique) during the AY 2017-2018, while the second author was a Distinguished Visiting Professor and the first author a visiting doctoral student at the Laboratoire de Mécanique des Solides. The work of the first and second authors was also supported in part by the National Science Foundation through grant DMS-1613753.

†Field of Theoretical and Applied Mechanics, Cornell University, Ithaca, NY 14853 (sp2328@cornell.edu).

‡Department of Mathematics and Field of Theoretical and Applied Mechanics, Cornell University, Ithaca, NY 14853 (tjh10@cornell.edu).

§Laboratoire de Mécanique des Solides, C.N.R.S. UMR7649 & Département de Mécanique, École Polytechnique, Institut Polytechnique de France, Palaiseau, France, and Aerospace Engineering Department & Mechanical Engineering Department (emeritus), The University of Michigan, Ann Arbor, MI (nicolas.triantafyllidis@polytechnique.edu).

subsequently carried out employing the full rectangular domain. Transverse wrinkled patterns of arbitrary phase—neither symmetric nor anti-symmetric, in general—were obtained. Again, these yield precisely the same global bifurcation diagram, independent of the phase. Moreover, as the phase is increased (or decreased) an entire closed orbit of computed solutions, connecting the symmetric and anti-symmetric patterns, is inferred. In other words, the system behaves as though it possesses a continuous symmetry group in the transverse direction.

Nonetheless, the complete symmetry group of the rectangular reference configuration in $\mathbb{R}^3$ is finite, and its irreducible representations are all 1-dimensional. Consequently, the physical symmetry of the problem does not account for the observed degeneracy. The question is "What does?" The wrinkling problem addressed in [1] is difficult to analyze. First, there is no closed-form trivial (planar) solution; a difficult problem of 2-dimensional nonlinear elasticity must be solved numerically. Worse, the domain has true corners; the solutions are not classical. Therefore, a rigorous bifurcation analysis, much less an analysis of the above-mentioned behavior, is apparently out of reach. However, the apparent emergence of continuous symmetry in a problem possessing only a finite symmetry group, which is the primary motivation of this work, can be studied in a simple model that is amenable to analysis, viz., an axially compressed, linear beam on a softening, nonlinear elastic foundation.

Two-scale asymptotic approaches for beams resting on an elastic foundation or fluid supported beams are well known [6, 7, 8, 9, 10, 11, 12, 13]. For infinite-length beams these correspond to a one-parameter family of asymptotic solutions that rapidly decay at $\pm\infty$ [14, 15, 16, 17]. An arbitrary phase shift acting on the "fast" variable serves as the parameter, and an even solution connects to an odd one as the phase varies. Here we pursue the case of very long, simply supported finite-length beams. We treat these as a perturbation from the infinite-length case. Intuitively one expects the correction to approach zero as the length approaches infinity. Our main contribution here is that we obtain an additive correction term that is an exponentially decaying function of the length. Accordingly, we deduce, for sufficiently long beams, that all phase shifts acting on the fast variable yield equivalent solutions modulo exponentially small terms. We refer to this as *hidden asymptotic symmetry*. Clearly the exponentially small correction terms are not detectable by numerical methods for sufficiently long beams. We illustrate this via finite-element solutions of the boundary value problem which show excellent agreement with the asymptotic solution. In the same way, we deduce that the energy difference between phase-shifted solutions is exponentially small. We compute global bifurcation diagrams, verifying that the corrected asymptotic solutions coincide with secondary bifurcations for very long beams of finite length. The numerically calculated bifurcation diagram can be validated through a complete local bifurcation analysis near the bifurcation points. A discussion to this end is provided in Appendix A, which extends the work in [8] for secondary bifurcation points.

The outline of the work is as follows. After briefly summarizing a nondimensional formulation for the problem in section 2, we provide the main results of this work in section 3. We first summarize the existence of nontrivial solutions bifurcating from the compressed straight state. These solutions can be identified with spatially periodic solutions that are even and odd, respectively, for lengths that are odd and even multiples of π, respectively. We then focus on amplitude modulated solutions from the primary path of odd-periodic solutions (modulated solutions from the even-periodic solutions follow in the same manner). Following the lead of [7], we seek two-scale solutions and obtain the so-called amplitude equation. We analyze the amplitude

equations, obtaining an asymptotic correction to the infinite-length solution for the very long, simply supported beams.

In section 4 we present finite-element solutions for sufficiently long beams, demonstrating the accuracy of the asymptotic solutions and the numerical equivalence of all phase-shifted solutions, as described above. We compute an apparent closed orbit of solutions connecting odd to even solutions; i.e., the numerical model behaves as though it possesses a continuous symmetry group. We conclude with some final remarks in section 5.

2. Beam on a nonlinear elastic foundation. We consider a linear elastic beam on a nonlinear elastic foundation, characterized by a softening cubic nonlinearity. The simply supported beam has length $\bar{L}$ and bending stiffness EI. The $\bar{x}$-axis coincides with the undeformed centerline of the beam, with origin at mid-span. The beam is subjected to axial, compressive end loading P, and we denote the small transverse displacement of the beam by $\bar{w}(\bar{x})$. The total potential energy of the system is given by

$$\bar{\mathcal{E}}[\bar{w}] = \int_{-\bar{L}/2}^{\bar{L}/2} \left[\frac{1}{2} EI \left(\frac{d^2\bar{w}}{d\bar{x}^2} \right)^2 - \frac{1}{2} P \left(\frac{d\bar{w}}{d\bar{x}} \right)^2 + \frac{1}{2} k_2 \bar{w}^2 - \frac{1}{4} k_4 \bar{w}^4 \right] d\bar{x}. \tag{2.1}$$

We rescale via $x = \bar{x}/L_c$, $w = \bar{w}/L_c$, and $L = \bar{L}/L_c$, where $L_c := (EI/k_2)^{1/4}$ is chosen as a characteristic length. The nondimensional potential energy functional, $\mathcal{E} := \bar{\mathcal{E}} L_c/EI$, then reads

$$\mathcal{E}[w] = \int_{-L/2}^{L/2} \left[\frac{1}{2} \left(w'' \right)^2 - \frac{\lambda}{2} \left(w' \right)^2 + \frac{1}{2} w^2 - \frac{1}{4} w^4 \right] dx, \tag{2.2}$$

where $(\cdot)' := \frac{d(\cdot)}{dx}$, $\lambda := \frac{P}{\sqrt{k_2 EI}}$, and $k_4 \equiv k_2 \sqrt{\frac{k_2}{EI}}$.

We observe here that the nondimensional length L being sufficiently large corresponds to a variety of scenarios, including the case that the thickness of the beam is sufficiently small (causing I to be sufficiently small) and/or the foundation stiffness k_2 is sufficiently large.

3. Asymptotic analysis. The first variation of the energy (2.2) leads to the equilibrium equation

$$w'''' + \lambda w'' + w - w^3 = 0, \tag{3.1}$$

on $(-L/2, L/2)$, subject to the boundary conditions

$$w(\pm L/2) = w''(\pm L/2) = 0. \tag{3.2}$$

The linearization of (3.1) about the trivial solution is given by

$$T(\lambda) w := w'''' + \lambda w'' + w = 0, \tag{3.3}$$

subject to (3.2). We focus here on two possible families of nontrivial solutions of the linearized problem, each at $\lambda = 2$:

Symmetric:

$$L = L_s := (2n-1)\pi, n = 1, 2, \ldots; \; w = h_s := \sqrt{\frac{2}{L_s}} \cos(x). \tag{3.4}$$

Anti-symmetric:

$$L = L_a := 2n\pi, n = 1, 2, \ldots; \; w = h_a := \sqrt{\frac{2}{L_a}}\sin(x). \tag{3.5}$$

In Appendix A we demonstrate that these correspond to subcritical pitchfork bifurcations.

We now proceed to derive amplitude modulated asymptotic solutions considering $L = L_a$ in a small half-neighborhood of $\lambda = 2$. In particular, we choose $\varepsilon = \sqrt{2-\lambda}$, and (following [7]) seek a two-scale solution of the form

$$w_a = \varepsilon A(X)\sin(x), \tag{3.6}$$

where $X = \varepsilon x$. It will soon be clear that a similar analysis can be carried out for w_s with $L = L_s$. In any case, (3.6) and the boundary conditions (3.2) imply that

$$\frac{dA}{dX}\,|_{X=\pm\frac{\varepsilon L_a}{2}} = 0. \tag{3.7}$$

Next we substitute (3.6) into the energy (2.2). To leading order in ε, integration by parts and (3.7) yield

$$\mathcal{E}_a[A] = \varepsilon^3 \int_{-\frac{\varepsilon L_a}{2}}^{\frac{\varepsilon L_a}{2}} \left[\left(\frac{dA}{dX}\right)^2 + \frac{1}{4}A^2 - \frac{3}{32}A^4\right] dX, \tag{3.8}$$

the first variation of which delivers the amplitude equation

$$\frac{d^2A}{dX^2} - \frac{1}{4}A + \frac{3}{16}A^3 = 0. \tag{3.9}$$

The general solution of (3.9) can be expressed in terms of the Jacobi elliptic "dn" function, viz.,

$$A(X) = \alpha\ \mathrm{dn}(\Omega X, m), \quad m \in [0, 1). \tag{3.10}$$

Our goal here is to obtain an asymptotic approximation of A as the length of the beam becomes very large but stays finite. Substituting (3.10) into (3.9), we find

$$\alpha = 2\sqrt{\frac{2}{3(2-m)}}, \quad \Omega = \frac{1}{2\sqrt{2-m}}. \tag{3.11}$$

Next we use the boundary conditions (3.7) to deduce

$$\alpha\ m\ \Omega\ \mathrm{sn}\left(\frac{\varepsilon\Omega L_a}{2}\right)\ \mathrm{cn}\left(\frac{\varepsilon\Omega L_a}{2}\right) = 0. \tag{3.12}$$

At $m = 0$, $\mathrm{dn}(\Omega X, 0) \equiv 1$, and from (3.9), (3.11), the amplitude reduces to $A \equiv 2/\sqrt{3}$, which we recall represents the primary bifurcating path; cf. after (A.6). Thus, we require $m \in (0, 1)$ for secondary bifurcation. With this in hand ($m \neq 0$), (3.12) implies that the argument of sn or cn is equal to a quarter period, viz.,

$$\varepsilon\Omega L_a = 2K(m), \tag{3.13}$$

where

$$K(m) = \int_0^{\pi/2} \frac{1}{\sqrt{1 - m\sin^2\phi}} d\phi; \tag{3.14}$$

cf. [18]. We note here that $K(m) \longrightarrow \infty$ as $m \nearrow 1$.

We now fix the $\varepsilon > 0$ sufficiently small and seek an expression for L_a. From (3.11) and (3.13) we find

$$L_a = f(\mu) := \frac{4\sqrt{1+\mu}}{\varepsilon} K(1-\mu), \tag{3.15}$$

where $\mu := 1 - m, \mu \in (0, 1)$, is the complementary modulus. From (3.15) and the behavior of K, we see that

$$f \longrightarrow \infty \text{ as } \mu \searrow 0, \quad \text{and } f(1) = \frac{2\sqrt{2}\pi}{\varepsilon}. \tag{3.16}$$

Moreover, we deduce

$$\frac{df}{d\mu} = g(\mu), \tag{3.17}$$

where

$$g(\mu) = -\frac{2}{\varepsilon\mu\sqrt{1+\mu}} \int_0^{\pi/2} \frac{\cos^2(\phi) - \mu\sin^2(\phi)}{\sqrt{\cos^2(\phi) + \mu\sin^2(\phi)}} d\phi < 0, \tag{3.18}$$

i.e., f is monotonically decreasing. The above observations can be verified by plotting f as a function of μ for fixed values of ϵ as shown in Figure 1.

Hence, (3.16)–(3.18) imply there is a unique value $\mu \in (0, 1)$ for every

$$L_a > \frac{2\sqrt{2}\pi}{\varepsilon}; \tag{3.19}$$

i.e., secondary solutions exist. We note that at criticality (equality), (3.19) gives

$$\epsilon_c = 2\sqrt{2}\pi/L_a \implies \lambda_c = 2 - 2(2\pi/L_a)^2. \tag{3.20}$$

Of course (3.15)–(3.18) also imply that $\mu = f^{-1}(L_a)$, where f^{-1} is monotonically decreasing for $L_a \in (\frac{2\pi\sqrt{2}}{\varepsilon}, \infty)$, with $f^{-1}(\frac{2\pi\sqrt{2}}{\varepsilon}) = 1$ and $f^{-1} \searrow 0$ as $L_a \longrightarrow \infty$. Accordingly, we seek an asymptotic solution of (3.15) in the limit as μ goes to zero. From [18] we observe that K (cf. (3.14)) has a logarithmic singularity at $\mu = 0$, from which we deduce

$$L_a = f(\mu) \sim \frac{2}{\varepsilon} \ln\left(\frac{16}{\mu}\right) \text{ as } \mu \searrow 0 \Longrightarrow \mu \sim 16 \exp\left(-\frac{\varepsilon L_a}{2}\right) \text{ as } L_a \longrightarrow \infty. \tag{3.21}$$

We now obtain an asymptotic expression for $A(X)$ from (3.10) when μ is close to zero. Define $A^*(X) := \lim_{\mu\searrow 0} [\alpha \text{ dn}(\Omega X, \mu)]$. Noting that $\lim_{\mu\searrow 0} \alpha(\mu) = 2\sqrt{2/3}$ and $\lim_{\mu\searrow 0} \Omega(\mu) = 1/2$, one obtains

$$A^*(X) = 2\sqrt{\frac{2}{3}} \text{dn}\left(\frac{X}{2}, \mu \searrow 0\right). \tag{3.22}$$

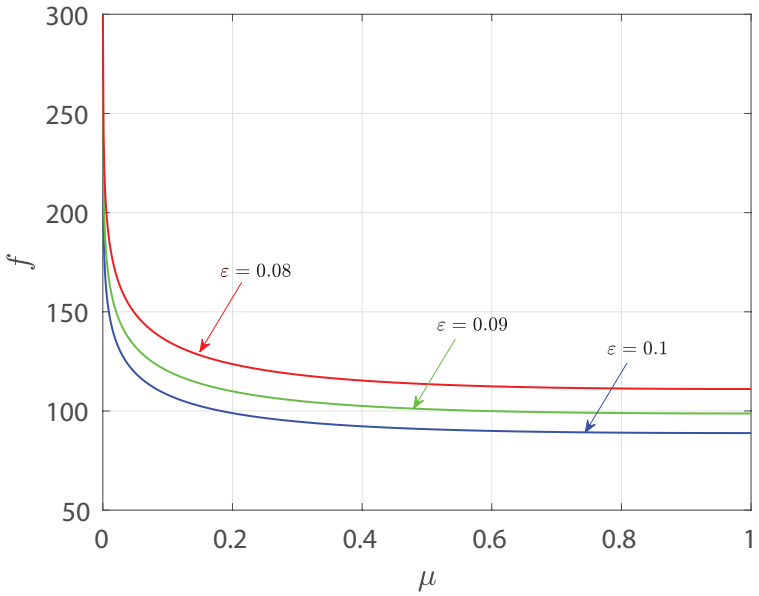

FIG. 1.

The dn(X/2, μ) function can be approximated in terms of hyperbolic functions when μ is close to zero [18], in which case $A^*(X)$ has an asymptotic expression given by

(3.23)
$$A^*(X) \sim 2\sqrt{\frac{2}{3}}\,\operatorname{sech}\left(\frac{X}{2}\right)\left[1+\frac{\mu}{4}\left\{\sinh\left(\frac{X}{2}\right)\cosh\left(\frac{X}{2}\right)+\left(\frac{X}{2}\right)\right\}\tanh\left(\frac{X}{2}\right)\right].$$

Finally, on substituting μ from (3.21) into (3.23), we get

(3.24)
$$A^*(X) \sim 2\sqrt{\frac{2}{3}}\,\operatorname{sech}\left(\frac{X}{2}\right) \times\left[1+4\exp\left(-\varepsilon L_a/2\right)\left\{\sinh\left(\frac{X}{2}\right)\cosh\left(\frac{X}{2}\right)+\left(\frac{X}{2}\right)\right\}\tanh\left(\frac{X}{2}\right)\right].$$

If we begin as in (3.6), but now with the symmetric ansatz $w_s = \varepsilon A(X)\cos(x)$ for $L = L_s$ (cf. (3.4)), it is not hard to see that the amplitude equation (3.9) is unchanged on the domain $(-L_s/2, L_s/2)$. Likewise, the boundary conditions (3.7) hold at $X = \pm\varepsilon L_s/2$. Moreover, an analysis identical to that given here in section 3 gives the same asymptotic expression (3.24) for the amplitude, but with L_s in place of L_a. Of course, these two amplitude functions have the same limit as $L_s, L_a \to \infty$, viz.,

(3.25)
$$A^*(X) \to 2\sqrt{\frac{2}{3}}\,\operatorname{sech}\left(\frac{X}{2}\right),$$

which confirms the fact that an infinitely long beam admits a one-parameter family

of solutions

$$w_{\infty,\phi} = 2\varepsilon\sqrt{\frac{2}{3}}\,\mathrm{sech}\left(\frac{X}{2}\right)\sin\left(x-\phi\right), \quad \phi \in [0, 2\pi). \tag{3.26}$$

Our goal is to show that this is essentially the case for extremely long beams as well.

We start with a beam of length $L_a = 2n\pi$, for very large values of n, and consider the asymptotic solution $w_a(x) = \varepsilon A^*(X)\sin(x)$, with $\varepsilon = \sqrt{2-\lambda}$ sufficiently small and fixed. In the view of (3.7), w_a satisfies the boundary conditions (3.2). Now define

$$w_{a,\phi} = \varepsilon A^*(X)\sin\left(x-\phi\right), \quad \phi \in [0, 2\pi), \tag{3.27}$$

which is also an asymptotic solution that does not satisfy the boundary conditions unless $\phi = 0$. However, for sufficiently large values of L_a (or n), (3.24) yields

$$\begin{aligned} w_{a,\phi}\left(x=\frac{L_a}{2}\right) &\sim 2\varepsilon\sqrt{\frac{2}{3}}\,\mathrm{sech}\left(\varepsilon\frac{L_a}{4}\right)\sin\left(\frac{L_a}{2}-\phi\right) \\ &\times\left[1+4\exp\left(-\varepsilon L_a/2\right)\left\{\sinh\left(\varepsilon\frac{L_a}{4}\right)\cosh\left(\varepsilon\frac{L_a}{4}\right)+\left(\varepsilon\frac{L_a}{4}\right)\right\}\tanh\left(\varepsilon\frac{L_a}{4}\right)\right] \\ &= 2\varepsilon\sqrt{\frac{2}{3}}\,\mathrm{sech}\left(\varepsilon\frac{L_a}{4}\right)\sin\left(\frac{L_a}{2}-\phi\right) \\ &\times\left[2+\exp\left(-\varepsilon L_a\right)+\exp\left(-\varepsilon L_a/2\right)\left(\varepsilon L_a\tanh\left(\varepsilon\frac{L_a}{4}\right)-2\right)\right] \end{aligned} \tag{3.28}$$

with a similar expression resulting at $x = -L_a/2$. That is, for $\phi \neq 0$, the end displacements miss satisfying the boundary conditions by exponentially small terms only. Clearly, we can start with $w_s(x) = \varepsilon A^*(X)\cos(x)$ and make the same argument for $w_{s,\phi}(x) = \varepsilon A^*(X)\cos(x-\phi)$, for an arbitrary phase shift ϕ, and arrive at the same conclusion for very large L_s.

In a similar manner, we substitute (3.10) into (3.8) to obtain an asymptotic expression for the potential energy:

$$\begin{aligned} \mathcal{E}_a = \frac{2\varepsilon^3}{3}\int_{-\frac{\varepsilon L_a}{2}}^{\frac{\varepsilon L_a}{2}}\Bigg[&\frac{m^2}{(2-m)^2}\mathrm{sn}^2(\Omega X,m)\ \mathrm{cn}^2(\Omega X,m) \\ &+\frac{1}{(2-m)}\mathrm{dn}^2(\Omega X,m)-\frac{1}{(2-m)^2}\mathrm{dn}^4(\Omega X,m)\Bigg]dX. \end{aligned} \tag{3.29}$$

Since the integrand of $\mathcal{E}_a$ is even, the energy can be rewritten via the change of variable $\Omega X = t$, which yields

$$\begin{aligned} \mathcal{E}_a = \frac{8\varepsilon^3}{3}\int_0^{\frac{\varepsilon\Omega L_a}{2}}\Bigg[&\frac{m^2}{(2-m)^{\frac{3}{2}}}\mathrm{sn}^2(t)\ \mathrm{cn}^2(t)+\frac{1}{(2-m)^{\frac{1}{2}}}\mathrm{dn}^2(t) \\ &-\frac{1}{(2-m)^{\frac{3}{2}}}\mathrm{dn}^4(t)\Bigg]dt. \end{aligned} \tag{3.30}$$

We now substitute $m = 1-\mu$ into the expression of the total potential energy $\mathcal{E}_a$ given in (3.30) and then expand the integrand in a Taylor series centered around $\mu = 0$. On

approximating the functions sn(t), cn(t), and dn(t) in terms of hyperbolic functions for $\mu \searrow 0$ [18] and neglecting the terms of order μ^2 and higher, we find

$$\mathcal{E}_a^* \sim \mathcal{E}_\infty + \mathcal{E}_{L_a}, \tag{3.31}$$

where

$$\mathcal{E}_\infty = \varepsilon^3 \left(\frac{8}{3}\right) \int_0^{\frac{\varepsilon\Omega L_a}{2}} \frac{2\,\sinh^2(t)}{\cosh^4(t)} dt = \varepsilon^3 \left(\frac{16}{9}\right), \tag{3.32}$$

and

$$\begin{aligned} \mathcal{E}_{L_a} &= \varepsilon^3\ \mu \left(\frac{8}{3}\right) \int_0^{\frac{\varepsilon\Omega L_a}{2}} \left[\frac{t\,\sinh(t)}{\cosh^3(t)} - \frac{2\ t\,\sinh(t)}{\cosh^5(t)} + \frac{5}{\cosh^4(t)} - \frac{4}{\cosh^2(t)}\right] dt \\ &= -\varepsilon^3 \exp\left(-\varepsilon L_a/2\right) \left(\frac{4}{3}\right). \end{aligned} \tag{3.33}$$

Here $\mathcal{E}_\infty$ corresponds to the energy of an infinitely large beam, and $\mathcal{E}_{L_a}$ represents the energy correction owing to the finiteness of the beam length. For a symmetric ansatz $w_s = \varepsilon A(X)\cos(x)$ with $L = L_s$, it can be shown that the asymptotic expression for energy is identical to (3.31), with $L = L_s$. When $L_a, L_s \to \infty$, $\mathcal{E}_{L_a} = \mathcal{E}_{L_s} = 0$, and we recover the energy of an infinitely long beam. Moreover, the energy of the asymptotic solution $w_{a,\phi}$ can be obtained by substituting (3.27) into (2.2). Noting that $A^*(X)$ satisfies (3.7) at the boundaries $x = \pm L_a/2$, we see that an integration of (2.2) by parts gives the leading order terms

$$\mathcal{E}_{a,\phi} \sim -\varepsilon^2 \left[\frac{\left(A^*\left(\varepsilon x\right)\right)^2 \sin\left(2\left(x-\phi\right)\right)}{2}\right] \Bigg|_{-\frac{L_a}{2}}^{\frac{L_a}{2}} + \mathcal{E}_a, \tag{3.34}$$

where $\mathcal{E}_a$ is the energy of the anti-symmetric configuration; cf. (3.8). We observe that the boundary terms in (3.34) are exponentially small for fixed, small $\varepsilon > 0$ and L_a sufficiently large; cf. (3.24). That is, the energies of beam configurations (3.27) differ by exponentially small terms for very long length beams.

Remark. As special cases of (3.34), the energies of the anti-symmetric ($\phi = 0, \pi$) and the symmetric ($\phi = \pi/2, 3\pi/2$) configurations are recovered. Observe that each of these differ from the energy of an infinitely long beam by terms exponentially small in beam length, as was conjectured in [16].

4. Comparison with numerical solutions. The objectives of this section are twofold: (1) We present numerical bifurcation results, employing a finite-element model for long beams, with the goal of validating the asymptotic results from the previous section. For the numerical computation, we first consider beam lengths of 40π and 50π in the anti-symmetric case, and lengths of 45π and 55π in the symmetric case, which are in consonance with (3.4), (3.5). In choosing these, we note that the asymptotic results of section 3 give strong evidence for the existence of modulated, two-scale solutions for sufficiently small values of the parameter $\varepsilon = \sqrt{2-\lambda}$. (2) Later in the section we demonstrate that for a fixed small parameter ε, one can choose an appropriate beam length (cf. discussion following Table 2) for which a continuous orbit of solutions parametrized by the phase angle can be computed. The beam lengths so obtained are an order of magnitude larger than the lengths previously considered.

For the discretized model we use cubic Hermite shape functions to approximate the displacement of the beam at the element level, and we employ 10 elements for every π units of length. Furthermore, we exploit anti-symmetry and symmetry in the numerical calculations. In particular, we consider the system on the interval $(0, L/2)$, with a simple support at $x = L/2$, with the following essential boundary conditions at $x = 0$:

$$\begin{aligned} &\text{Anti-symmetric case: } w(0) = 0; \\ &\text{Symmetric case: } w'(0) = 0. \end{aligned} \tag{4.1}$$

We use pseudo–arc-length continuation [19] to compute numerical solution paths. We first obtain the primary bifurcation path, corresponding to a subcritical bifurcation, as depicted in Figure 2, where $\xi = \max|w|$ denotes the maximum displacement. All solutions along that path are (extendable to) periodic solutions on the entire x-axis. For that reason the solution paths for each of our chosen lengths plot the same in Figure 2. Next we compute secondary bifurcating solution paths. We pinpoint the locations of secondary bifurcation points by monitoring the occurrence of a zero eigenvalue of the tangent stiffness matrix, and then we employ a standard branch-switching technique [19] to get onto the secondary bifurcating solution path. We note that the primary and the secondary bifurcating branches are all subcritical, indicating unstable equilibria.

The secondary bifurcation points corresponding to the four lengths are shown as open circles in Figure 2. Their computed values are summarized in Table 1 along with their respective values as predicted by the asymptotic analysis, viz., $\lambda_c = 2 - 8\pi^2 {L_\alpha}^2 (\alpha = \text{a or s})$; cf. (3.19) (and the discussion that immediately follows). The agreement is clearly excellent.

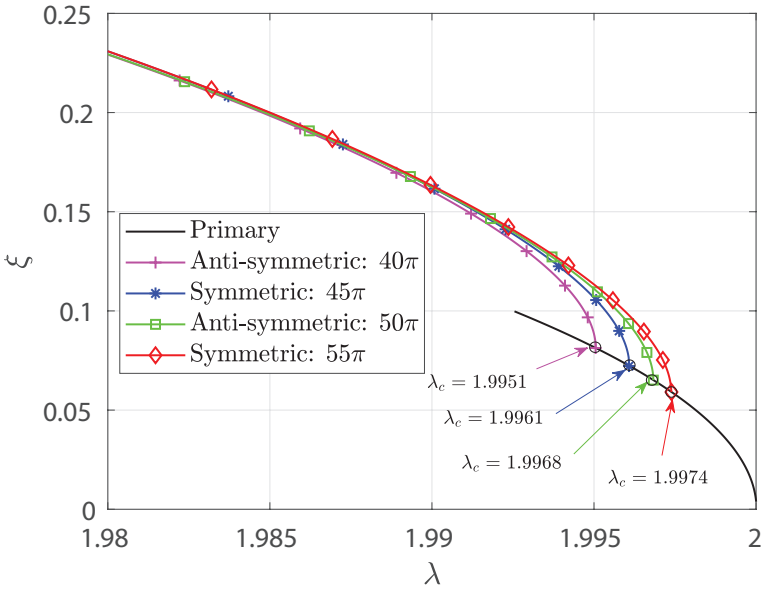

FIG. 2. $\xi = max|w|$ *versus* $\lambda =$ *load.*

TABLE 1
Secondary critical loads.

Beam length	Analytical	Numerical
40π	1.9950	1.9951
45π	1.9960	1.9961
50π	1.9968	1.9968
55π	1.9974	1.9974

In Table 2 we list the computed values of the total potential energy for the lengths considered along with their respective asymptotic values from (3.31)–(3.33). Aside from the very good agreement, we observe that the difference between the asymptotic energy and the numerically calculated energy decreases with an increase in beam lengths.

TABLE 2
Energy per unit beam length.

Beam length	Analytical (10^{-5})	Numerical (10^{-5})	% difference
40π	1.4091	1.3719	2.71
45π	1.2658	1.2473	1.49
50π	1.1296	1.1186	0.98
55π	1.0357	1.0280	0.75

Figures 3 and 4 provide a comparison of the beam deformation calculated using finite-element method and the asymptotic analysis, viz., $w(x) = \varepsilon A^*(X)\ p(x)$, ($p(x) = \sin(x)$ or $\cos(x)$) for anti-symmetric and symmetric modes, respectively, at $\varepsilon = 0.1$, which corresponds to $\lambda = 1.99$ in Figure 2. Once again, the agreement between the numerical results and the asymptotic solutions is excellent.

We now proceed to compute an apparent one-parameter family of solutions corresponding to arbitrarily phase-shifted deformations of the beam for extremely long beams (cf. section 3) using the finite-element model and a beam length of $L = L_a$. For this we require longer lengths of the beam than the four cases considered above. We explain this below.

The asymptotic amplitude function (3.24) takes a maximum value at $X = 0$ for $X \in [-\varepsilon L_a/2, \varepsilon L_a/2]$ and decreases towards $X = \pm\varepsilon L_a/2$. Furthermore, we see from (3.28) that $w_{a,\phi}$ misses the zero-displacement boundary conditions at most by $\tilde{w} := \max_{\phi\in[0,2\pi)} w_{a,\phi}(\pm L_a/2) = \varepsilon A^*(\varepsilon L_a/2)$. Clearly, if we choose $L_a = 2n\pi$ large enough so that $\tilde{w} \approx 0$, say, for $\varepsilon = 0.1$, it would ensure that the simply supported boundary conditions are satisfied for any phase angle $\phi \in [0, 2\pi)$. Accordingly, we choose $L_a = 200\pi$, which gives $\tilde{w} = \mathcal{O}(10^{-8})$. It is worth mentioning that this estimate for $\tilde{w}$ was obtained merely to choose a sufficiently long beam for the purpose of demonstration. In fact, one could choose any long length beam which gives $\tilde{w} \approx 0$.

The numerically computed beam deformations are obtained by employing the asymptotic displacement function $w_{a,\phi}$ given in (3.27) as the initial trial solution for the discretized model at $\varepsilon = 0.1$. Newton's method is then used iteratively. For any chosen $\phi \in [0, 2\pi)$ the implementation converges within four iterations with a residue of the order $\mathcal{O}(10^{-13})$ using the default double-precision in MATLAB. Figure 5 gives a polar plot of the ℓ^2-norm as a function of ϕ (rational multiples: $\phi(p) := p\pi, p = 0, 1/24, \ldots, 47/24$; irrational multiples: $\phi(q) := q\pi, q = \sqrt{2}, \sqrt{3}, \sqrt{5}-2, \sqrt{7}-2, \sqrt{11}-2, \sqrt{13}-2$) for the numerically computed solution points which align exactly on a circle. Symmetric solutions correspond to $p = 12/24, 36/24$; anti-symmetric solutions

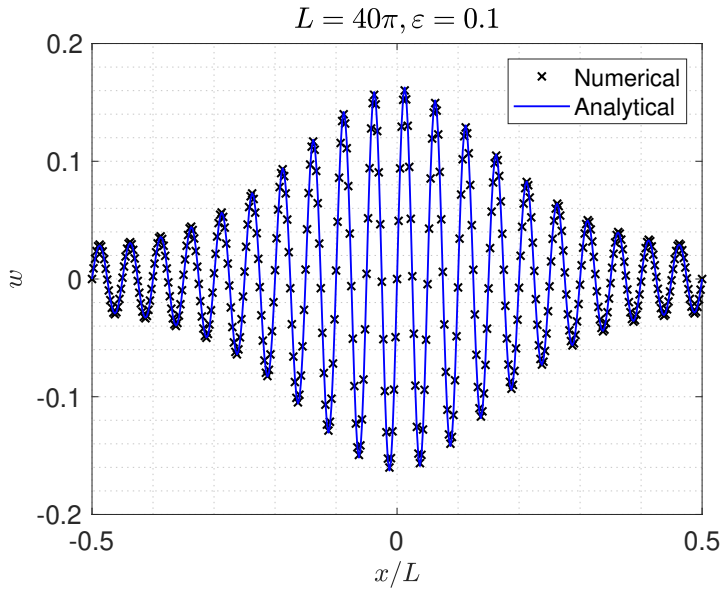

(a)

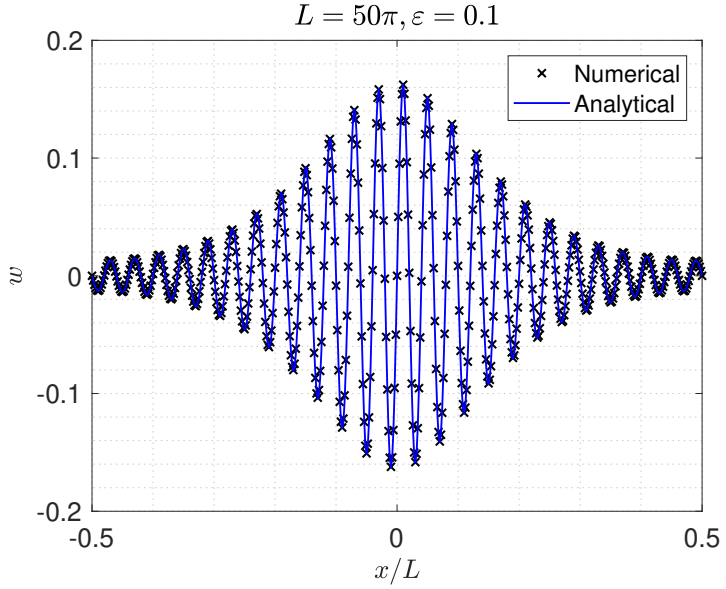

(b)

FIG. 3. *Comparison for anti-symmetric deformation modes.*

correspond to $p = 0, 24/24$; and all the other values of p and all values of q correspond to solutions that are neither even nor odd.

Remark. For the four lengths considered earlier (cf. Table 1), the solutions do not converge via the procedure mentioned above for any arbitrary ϕ (other than $\phi = 0$) because $\tilde{w} = \mathcal{O}(10^{-3})$ fails to accurately account for zero-displacement boundary

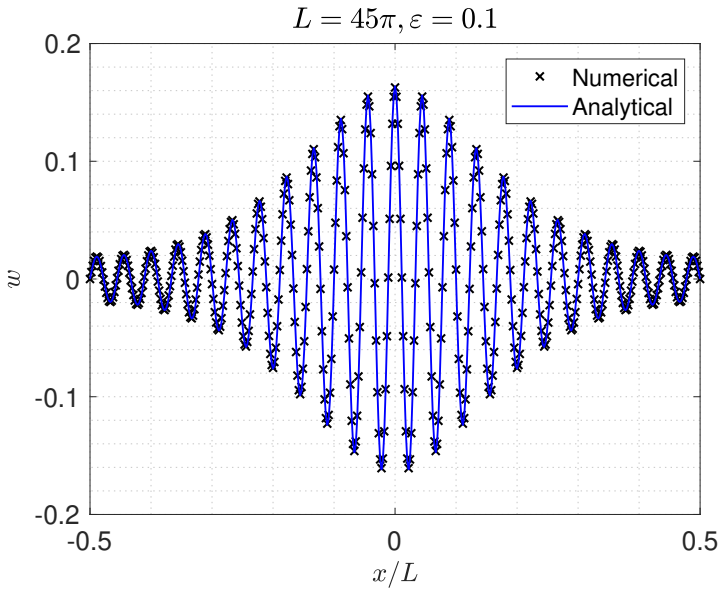

(a)

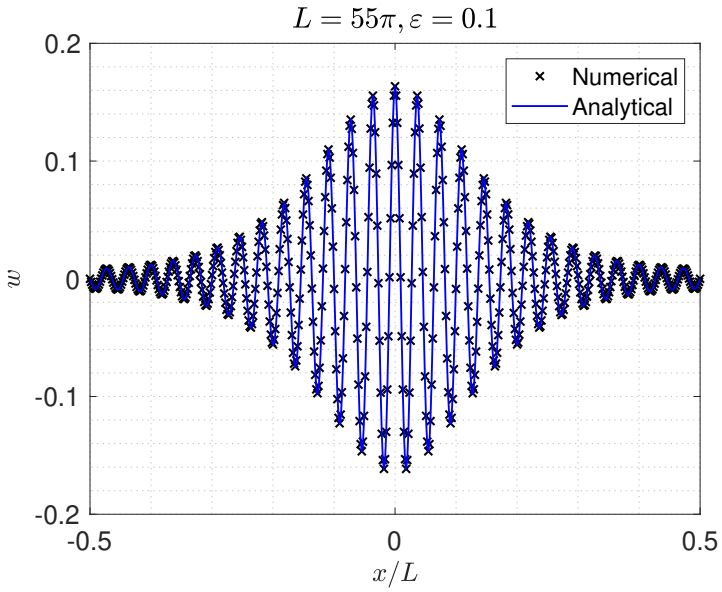

(b)

FIG. 4. *Comparison for symmetric deformation modes.*

conditions.

Figures 6 to 8 give a sampling of the numerical solutions of the beam displacement field obtained as described above.

5. Conclusion. As mentioned in the introduction, this work is motivated by the symmetry properties of the solution for wrinkling in highly stretched thin elastic

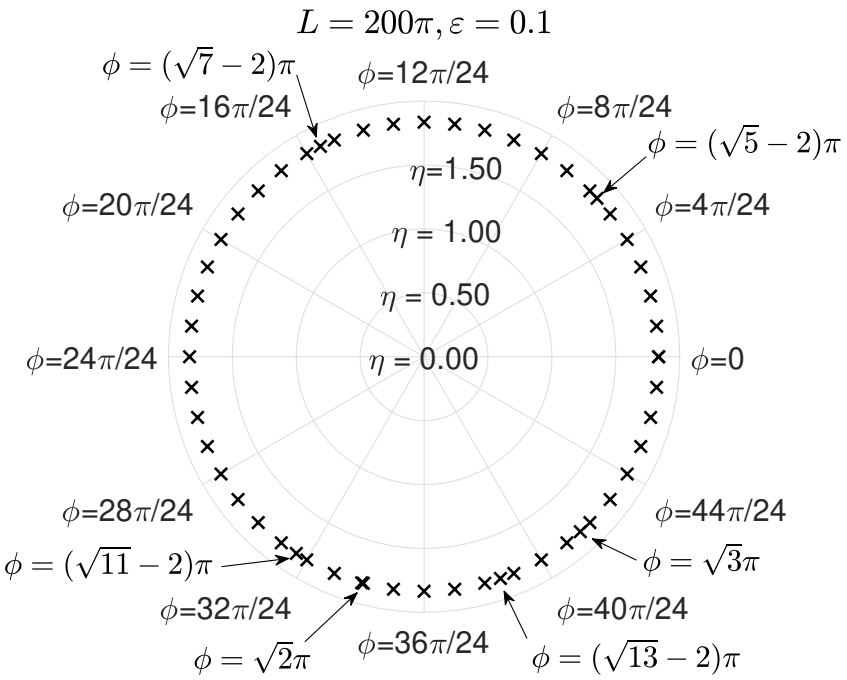

FIG. 5. $\eta = \|w_{a,\phi}\|_2$ *versus* $\phi =$ *phase-angle.*

membranes [1]. A direct comparison of our analysis here for the "long beam" problem with the more complex wrinkling problem is not possible. Nonetheless, both models exhibit the same phenomenon, viz., behavior associated with a continuous symmetry group in a computational problem possessing merely a finite symmetry group. In the beam problem, the latter corresponds to simple even-odd symmetry with respect to the origin. Yet, as the nondimensional length L becomes sufficiently large, an additional translation symmetry emerges asymptotically, viz., the correction to the infinite-length solution is an exponentially decaying function of the length.

Our results demonstrate the asymptotic emergence of an orbit of solutions in a problem having only a finite complete symmetry group. We mention that in the analysis of a closely related beam problem, an asymptotic correction to the exact infinite-length solution for sufficiently long finite beams is obtained in [17]. The construction there is based on an ansatz that is restricted to either symmetric or anti-symmetric solutions. In particular, asymptotic orbits of solutions are not addressed in that work.

Appendix A. Bifurcation analysis.

A.1. Primary bifurcation. We view system (3.1), (3.2) as defining a continuously differentiable mapping $F(\cdot)$ from all real numbers λ and all four-times continuously differentiable functions w on $[-L/2, L/2]$ that satisfy (3.2) into all continuously differentiable functions on $[-L/2, L/2]$ (with the usual maximum norms). Thus, system (3.1), (3.2) is equivalent to $F(\lambda, w) = 0$. Clearly the straight state $w \equiv 0$ gives a trivial solution, i.e., $F(\lambda, 0) \equiv 0$. The linear operator in (3.3), $T(\lambda) = D_w F(\lambda, 0)$, is the total (Fréchet) derivative of $F(\lambda, \cdot)$ evaluated at $w = 0$.

It is not hard to show that $T(\lambda)$ is self-adjoint, and the usual sufficient condition for bifurcation [20] at $(\lambda, w) = (2, 0)$ is satisfied, viz., $\langle h_\beta, T'(2)h_\beta\rangle \neq 0, \beta = s, a$,

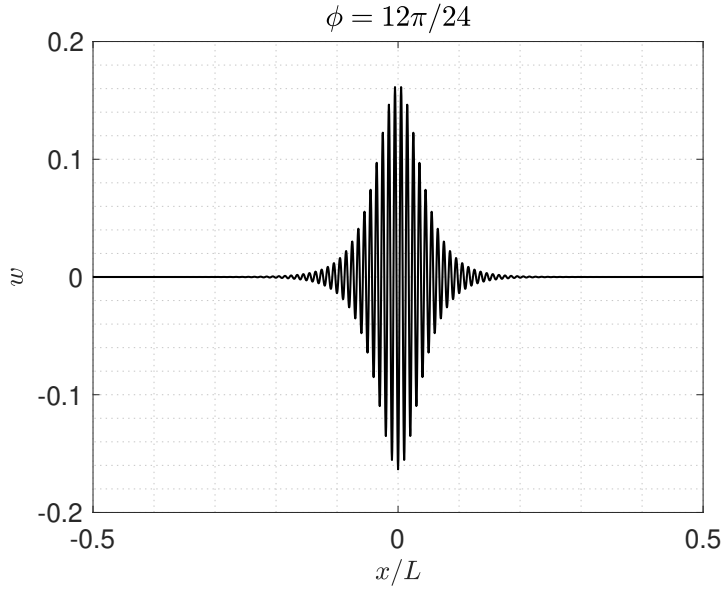

(a)

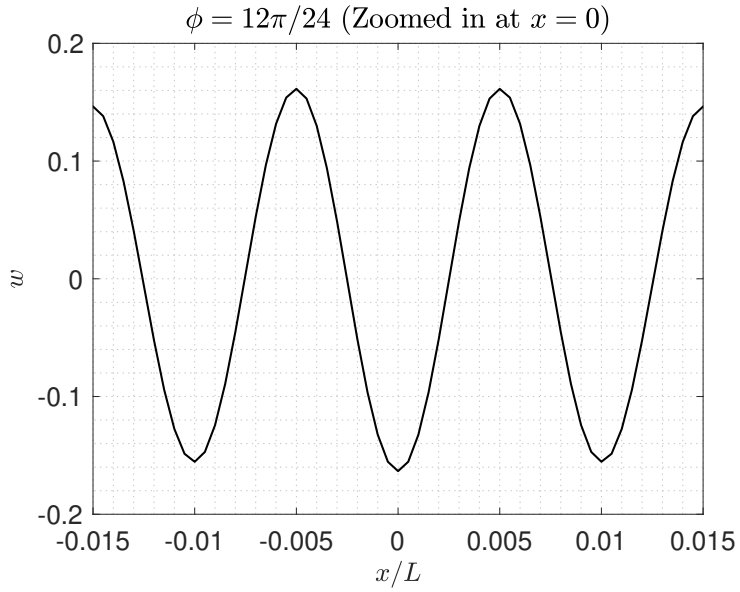

(b)

FIG. 6. *Symmetric.*

where $\langle f, g\rangle := \int_{-L/2}^{L/2} f(x)g(x)dx$. Accordingly, we deduce the existence of nontrivial solutions of (3.1), (3.2), and the usual Taylor-series expansion (e.g., [21]) reveals subcritical pitchfork bifurcations.

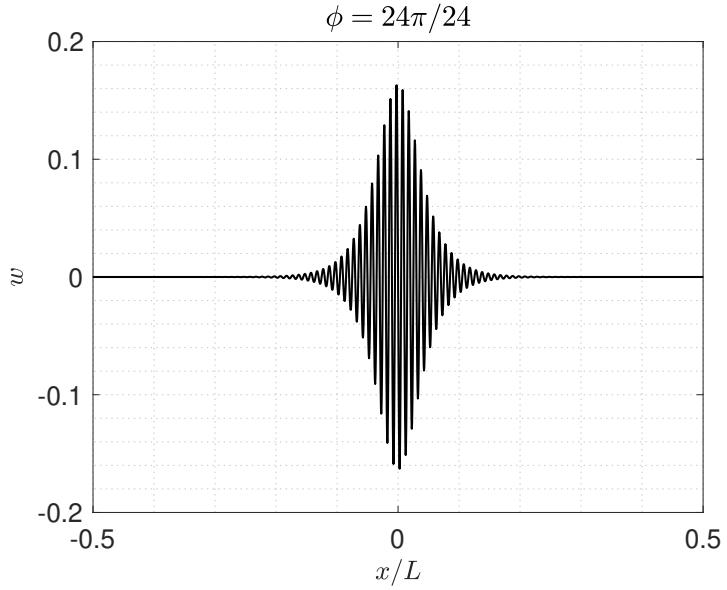

(a)

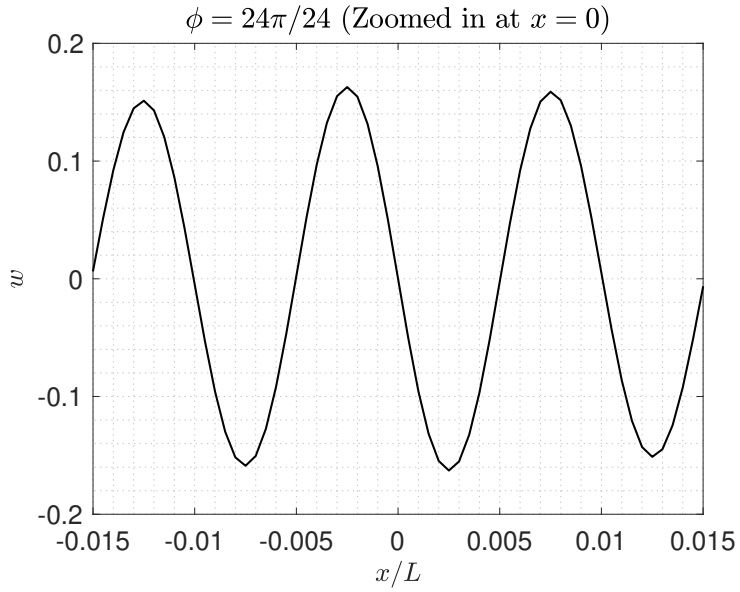

(b)

FIG. 7. *Anti-symmetric.*

Symmetric:

$$\lambda = 2 - \frac{3}{2L_s}\eta^2 + \mathcal{O}(\eta^4),\ w_s = \eta\sqrt{\frac{2}{L_s}}\cos(x) + \mathcal{O}(\eta^3);\ \eta := \langle h_s, w\rangle \to 0. \tag{A.1}$$

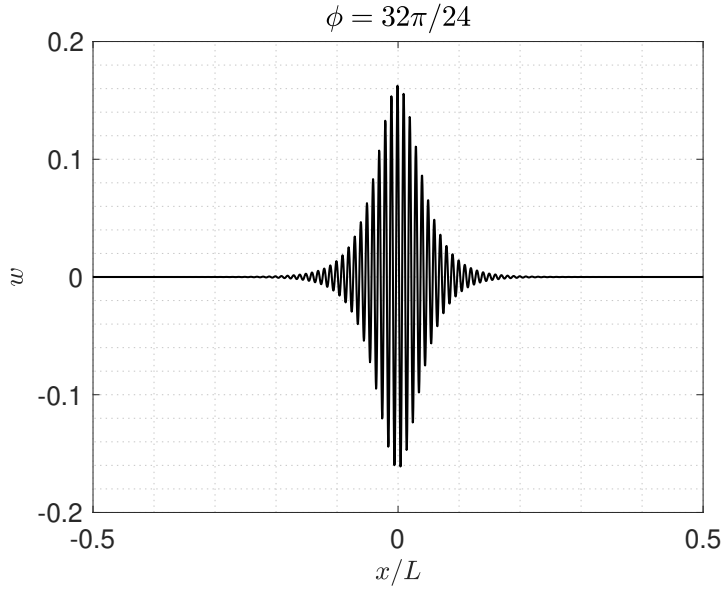

(a)

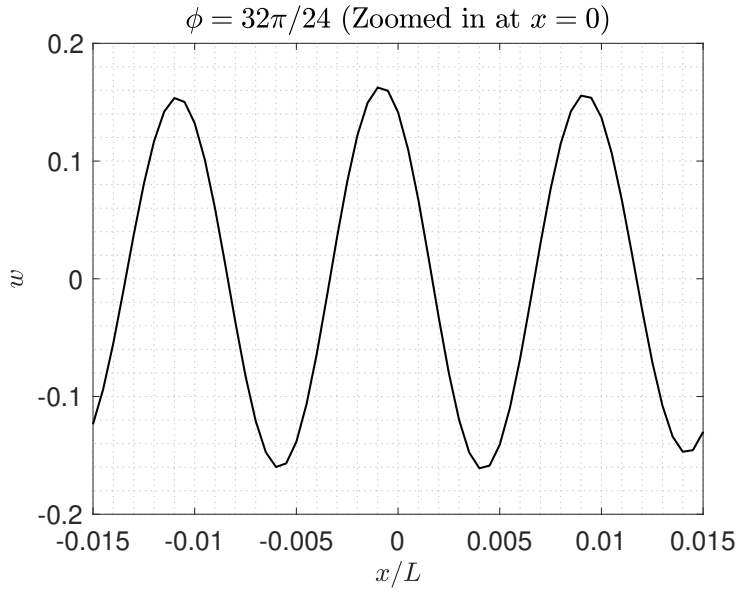

(b)

FIG. 8. *Neither symmetric nor anti-symmetric.*

Anti-symmetric:

$$\lambda = 2 - \frac{3}{2L_a}\eta^2 + \mathcal{O}(\eta^4),\ w_a = \eta\sqrt{\frac{2}{L_a}}\sin(x) + \mathcal{O}(\eta^3);\ \eta := \langle h_a, w\rangle \to 0. \tag{A.2}$$

A.2. Secondary bifurcation. We now obtain local bifurcating solutions of the amplitude equations, representing secondary bifurcation solutions of the boundary

value problem.

We return to the anti-symmetric case by considering $L = L_a$ with $\varepsilon = \sqrt{2-\lambda}$. A comparison of (A.2) with the two-scale anti-symmetric solution (3.6) implies that

$$\eta = \sqrt{\frac{2L_a}{3}}\varepsilon \Longrightarrow w_a = \varepsilon \frac{2}{\sqrt{3}} \sin(x) + \mathcal{O}(\varepsilon^3). \tag{A.3}$$

The trivial solution of (3.9) subject to (3.7) is a constant, say, A_o. Comparing (3.6) and (A.3), we see that $A_o = \frac{2}{\sqrt{3}}$, i.e., the primary branch of periodic solutions now appears as a constant (amplitude). We then look for a nontrivial solution of the form $A(\varepsilon x) = \frac{2}{\sqrt{3}} + u(x)$, which leads to the boundary value problem

$$u'' + \frac{(2-\lambda)}{2}\left(u + \frac{3\sqrt{3}}{4}u^2 + \frac{3}{8}u^3\right) = 0, \quad u'(\pm L_a/2) = 0. \tag{A.4}$$

Clearly $u \equiv 0$ is the trivial solution of (A.4), and the linearized problem is then given by

$$u'' + \frac{(2-\lambda)}{2}u = 0, \tag{A.5}$$

subject to the same boundary conditions (3.7). This problem admits the nontrivial solution $u = C\cos(\gamma_k x)$, where $\gamma_{k,a} := \frac{2k\pi}{L_a}$, $k = 1, 2, \ldots$. The corresponding bifurcation values are $\lambda = 2 - 2(\gamma_{k,a})^2$, which match with (3.20). Then, as in the previous section, a Taylor-series expansion yields the following family of subcritical pitchfork bifurcating solution branches for (A.4):

$$\lambda = 2 - 2(\gamma_{k,a})^2 - \frac{9}{2L_a}(\gamma_{k,a})^2 \eta^2 + \mathcal{O}(\eta^3), u = \eta\sqrt{\frac{2}{L_a}}\cos(\gamma_{k,a}x) + \mathcal{O}(\eta^2), \tag{A.6}$$

as $\eta \to 0$, $k = 1, 2, \ldots$. Since $A(X) = \frac{2}{\sqrt{3}} + u(X/\varepsilon)$, we see that (A.6) represents a family of solutions of (3.7), (3.9) bifurcating from the constant solution $A_0 = \frac{2}{\sqrt{3}}$.

REFERENCES

[1] T. J. Healey, Q. Li, and R.-B. Cheng, *Wrinkling behavior of highly stretched rectangular elastic films via parametric global bifurcation*, J. Nonlinear Sci., 23 (2013), pp. 777–805, https://doi.org/10.1007/s00332-013-9168-3.

[2] N. Friedl, F. G. Rammerstorfer, and F. D. Fisher, *Buckling of stretched strips*, Comput. Struct., 78 (2000), pp. 185–190, https://doi.org/10.1016/S0045-7949(00)00072-9.

[3] E. Cerda, K. Ravi-Chandar, and L. Mahadevan, *Wrinkling of an elastic sheet under tension*, Nature, 419 (2002), pp. 579–580, https://doi.org/10.1038/419579b.

[4] N. Jacques and M. Potier-Ferry, *On mode localisation in tensile plate buckling*, C. R. Méc., 333 (2005), pp. 804–809, https://doi.org/10.1016/j.crme.2005.10.013.

[5] V. Nayyar, K. Ravi-Chandar, and R. Huang, *Stretch-induced stress patterns and wrinkles in hyperelastic thin sheets*, Int. J. Solids Struct., 48 (2011), pp. 3471–3483, https://doi.org/10.1016/j.ijsolstr.2011.09.004.

[6] C. G. Lange and A. C. Newell, *The post-buckling problem for thin elastic shells*, SIAM J. Appl. Math., 21 (1971), pp. 605–629, https://doi.org/10.1137/0121066.

[7] M. Potier-Ferry, *Amplitude modulation, phase modulation and localization of buckling patterns*, in Collapse: The Buckling of Structures in Theory and Practice, J. M. T. Thompson and G. W. Hunt, eds., Cambridge University Press, Cambridge, UK, 1983, pp. 149–159.

[8] M. Potier-Ferry, *Foundations of elastic postbuckling theory*, in Buckling and Post-Buckling, Lecture Notes in Phys. 288, Springer, Berlin, 1987, pp. 1–82, https://doi.org/10.1007/BFb0009197.

[9] G. W. Hunt, H. M. Bolt, and J. M. T. Thompson, *Structural localization phenomena and dynamical phase-space analogy*, Proc. Roy. Soc. London Ser. A, 425 (1989), pp. 245–267, https://doi.org/10.1098/rspa.1989.0105.

[10] G. W. Hunt and M. K. Wadee, *Comparative Lagrangian formulations for localized buckling*, Proc. Roy. Soc. London Ser. A, 434 (1991), pp. 485–502, https://doi.org/10.1098/rspa.1991.0109.

[11] G. W. Hunt, M. K. Wadee, and N. Shiacolas, *Localized elasticae for the strut on the linear foundation*, J. Appl. Mech., 60 (1993), pp. 1033–1038, https://doi.org/10.1115/1.2900971.

[12] B. Audoly, *Localized buckling of a floating elastica*, Phys. Rev. E, 84 (2011), 011605, https://doi.org/10.1103/PhysRevE.84.011605.

[13] O. Oshri, F. Brau, and H. Diamant, *Wrinkles and folds in fluid-supported sheet of finite size*, Phys. Rev. E, 91 (2015), 052408, https://doi.org/10.1103/PhysRevE.91.052408.

[14] H. Diamant and T. A. Witten, *Compression induced folding of a sheet: An integrable system*, Phys. Rev. Lett., 107 (2011), 164302, https://doi.org/10.1103/PhysRevLett.107.164302.

[15] M. Rivetti, *Non-symmetric localized fold of a floating sheet*, C. R. Méc., 341 (2013), pp. 333–338, https://doi.org/10.1016/j.crme.2013.01.005.

[16] H. Diamant and T. A. Witten, *Shape and symmetry of fluid supported elastic sheet*, Phys. Rev. E, 88 (2013), 012401, https://doi.org/10.1103/PhysRevE.88.012401.

[17] M. Rivetti and S. Neukirch, *The mode branching route to localization of the finite-length floating elastica*, J. Mech. Phys. Solids, 69 (2014), pp. 144–155, https://doi.org/10.1016/j.jmps.2014.05.004.

[18] M. Abramowitz and I. A. Stegun, *Handbook of Mathematical Functions*, Dover Publications, New York, 1972.

[19] H. B. Keller, *Lecture on Numerical Methods in Bifurcation Problems*, Tata Inst. Fund. Res. Lectures on Math. and Phys. 79, Springer, Berlin, 1987.

[20] M. G. Crandall and P. H. Rabinowitz, *Bifurcation from simple eigenvalues*, J. Funct. Anal., 8 (1971), pp. 321–340, https://doi.org/10.1016/0022-1236(71)90015-2.

[21] G. Iooss and D. D. Joseph, *Elementary Stability and Bifurcation Theory*, 2nd ed., Springer, New York, 1990.